Link sito dell'editore:
https://asmedigitalcollection.asme.org/solarenergyengineering/article-abstract/137/4/041012/379226/Performance-Evaluation-of-a-New-Type-of-Combined?redirectedFrom=fulltext
Link codice DOI: https://doi.org/10.1115/1.4030727

Citazione bibliografica dell'articolo: Colangelo, G., Romano, D., and Marco Tina, G. (August 1, 2015). "Performance Evaluation of a New Type of Combined Photovoltaic–Thermal Solar Collector." ASME. J. Sol. Energy Eng. August 2015; 137(4): 041012.

Performance Evaluation of a New Type of Combined Photovoltaic – Thermal Solar Collector

Gianpiero COLANGELO[1]
Dipartimento di Ingegneria dell'Innovazione – Università del Salento
Via per Arnesano - 73100 Lecce – Italy
gianpiero.colangelo@unisalento.it

Danilo ROMANO
Dipartimento di Ingegneria dell'Innovazione – Università del Salento
Via per Arnesano - 73100 Lecce – Italy
danilo.romano@unisalento.it

Giuseppe Marco TINA
Dipartimento di Ingegneria Elettrica Elettronica e dei Sistemi – Università di Catania
Viale Andrea Doria 6 – 95125 Catania – Italy
gtina@diees.unict.it

ABSTRACT

A thermal analysis of a new photovoltaic-thermal solar panel design, called TESPI, has been performed using RadTherm Thermoanalitics software. Combinations of different water flow rates and different panel configurations have been analyzed to determine which one produces best performance in terms of optimal PV efficiency and available thermal energy. Higher total panel efficiencies (thermal and electrical) were achieved in configurations utilizing the highest water flow rates, independently from the chosen configuration. However, high water flow rates translated into minimal net temperature differences between the PV/T panel inlet and outlet.

Keywords

Photovoltaic, Thermal Solar Collector, Heat recovery, RadTherm, Efficiency

[1] Corresponding author: gianpiero.colangelo@unisalento.it, tel.+390832297752, fax +390832297777

1. INTRODUCTION

The possibility of a hybrid system, merging thermal and photovoltaic (PV) modules, is very promising for simultaneous production of electrical and thermal power, offering several advantages. The average range of efficiency of a traditional PV panel is between 10% and 15%, thus the radiation not converted in electricity is reflected or converted into heat. Moreover, the solar thermal collectors convert solar radiation to heat with an efficiency of 50 – 60 %. The idea of photovoltaic thermal hybrid panels faces several problems: from the thermal panel point of view there is the aim of capturing heat with a good thermal insulation, but, on the other hand, this increases the panel temperature and the temperature of PV cells, decreasing the conversion efficiency of PV system.

The goal of increasing the efficiency of both systems has driven the development of innovative technologies. In particular the investigation on the potential performance of flat solar thermal collectors using nanofluids as innovative heat transfer fluids for solar energy applications has evaluated the possibility to augment the performance of heat transfer fluid in a study on diathermic oil based nanofluids [1].

Moreover, the use of nanofluids in traditional solar flat panel revealed some technical issues, due to the nanoparticles sedimentation [2]. The opportunity to recover heat on a PV system is contemplated in a rotary type regenerator by means of an experimental study of a burner with high temperature heat recovery system for thermophotovoltaic applications [3].

A review of the state of the art for the hybrid PV-thermal solar collectors has been developed by Chow [4]; analysis of problems, models and experimental results have been faced in the work done by Zondag et al. [5] and Douve de Vries et al. [6]. Kalogirou [7], using TRNSYS, modelled a PVT/w system, complete with water tank. Kalogirou and Tripanagnostopoulos [8] examined domestic PVT/w applications, executing simulation studies, which covered 12 cases with two types of PV modules (pc-Si and a-Si) in three cities: Nicosia in Cyprus, Athens in Greece, and Madison in USA. Using the same approach, Vokas et al. [9] performed a theoretical analysis of PVT/w application in heating and cooling systems in three cities with different climate: Athens, Heraklion and Thessaloniki. Chow et al. [10] carried out measurements on glazed and unglazed PVT/w collector systems, with a validated numerical model. Dubey and Tiwari [11] performed a theoretical model to analyse the thermal and electric energy yielded by PVT system in different operating conditions.

In particular the starting point of this work is represented by the solution, which seems particularly suitable for a simple construction and industrialization process, presented by Rosa-Clot et al. [12]. It consists in superimposing a layer of water to the PV panel. The water is used as heat transfer fluid that flows into a polycarbonate box. The rear part of the panel is covered with a layer of polyurethane, used as thermal insulation. This particular solution is called Thermal Electric Solar Panel Integration (TESPI).

In literature many exhaustive studies focused on modelling of thermal behavior in thermal solar collector are presented, but the combination of PV and a thermal

collector changes considerably the behavior of both, mainly due to the heat flux increase dictated by the presence of the PV panel [13]. It is important to evaluate features of both systems, analyzing thermal collector and PV system models.

There are several approaches to realize a thermal model of a solar collector. The first is the steady state approach. The equations describing the mathematical model, based on the conservation of physical quantities, are simplified to have a set of equations with a low computational effort. Hottel and Woertz [14], Hottel and Whillier [15] and Bliss et al. [16] considered these simple assumptions: thermal capacitances were not considered and a single value of overall collector heat loss coefficient was identified. It depended on collector properties, plate temperature and external conditions. Duffie and Beckham [17] improved this model, assuming one-dimensional heat transfer and mainly in the normal direction to the flow plane. They adopted the electrical analogy to describe the steady state of the solar collector used for evaluating the thermal performance, considering a longer time weather data period.

An evolution of the steady stated model is the dynamic lumped model. Close [18] used for the first time a dynamical numerical model by means of a lumped thermal capacitance, which represents the thermal capacitance of the elements consisting the collector. In general it consists in a n-point lumped model and each one of those consists of one energy balance differential equation, based on the steady state scheme. The main limitation of Close model is that it cannot represent the spatial temperature profile inside the collector. It causes errors in heat losses calculation and in the outlet heat transfer fluid temperature profile. Wijeysundera [19] developed a 2-point lumped

model, in which the solar collector is modelled as two-region: the absorber plate and the heat transfer fluid, and the cover plates lumped together in a single equivalent cover. According to Wijeysundera [19] the steady state approach gives suitable results when hourly averaged meteorological data is used. If the meteorological condition changes quickly, the transient approach is preferable. Morrison and Ranatunga [20] implemented a 3-point lumped model: cover, collector and fluid, whereas Fraisse et al. [21] proposed a model based on an electrical analogy, considering the temperature dependency of thermo-physical characteristics of the entire system.

A discretized thermal model constitutes the most recent approach and it is at the basis of numerical solution. The lumped model has been developed by Klein et al. [22], who considered the heat transfer fluid temperature variation along the collector. It is discretized as an unsteady energy balance for each point. This method is named “In-node model”. The thermal capacitance of the fluid is taken into account by Kamminga

[23], who developed a 3n node model: cover and heat transfer fluid. This model becomes a 4node model, adding the capacitance of the rear thermal insulation. The solution results from a set of linear partial differential equations, simplified and solved into ordinary partial differential equations by means of numerical Runge-Kutta method [24]. A numerical method was developed by Oliva et al. [25]: it is a 4n-node model, in which the thermal inertia of the components is contemplated and the heat transfer fluid is calculated solving the Navier-Stokes equations, with a finite volume approach. The model proposed by Villar et al. [26] comes from Oliva model. It is a 3D model, based on mass and energy finite balance equations. The not-uniform distribution of the incident

solar radiation and the heat gain/loss were taken into account by Wirtz et al. [27] to predict thermal efficiency of a Parabolic Trough Concentrator in a in a 3D model.

Generally speaking, a PV module thermal model should consider the contribution of radiation, convection and conduction in the energy balance of photovoltaic cells based on climate variables, but normally simplified expressions are used to calculate the operating temperature of a PV module. In this context, a brief discussion regarding the operating temperature of one-sun commercial grade silicon-based solar cells/modules and its effect upon the electrical performance of photovoltaic installations is presented in [28], where suitable tabulations are given for most of the known algebraic forms which express the temperature dependence of solar electrical efficiency and, equivalently, solar power. Jones [29] estimated in a no-steady state model the module temperature, taking into account module heat capacity, short and long wave radiation, convection heat transfer and electrical power generation. In order to predict the energy production Tina et al. [30] developed a mathematical model that is able to calculate the PV cells layer temperature as a function of ambient temperature, wind speed and direction, total irradiance, and relative humidity. The thermal and electrical model has been experimentally verified in their later work [31].

Bergene et al.[32] enhanced a hybrid PV model under steady state conditions, focused on radiation and electrical conversion, but weak concerning thermal behaviour. Zondag et al. [33, [34] proposed a model of a hybrid water collector, performing various experimental studies. They studied a free flow PV/Thermal collector with air and water flowing above PV cells, analysing a 3D dynamic model and three steady state models:

3D, 2D and 1D. The model, under steady state condition, is made up by a set of equations of heat balance for the entire system. Starting from Zondag et al. [33, [34], Assoa et al. [35] presented a bi-fluid hybrid collector, where a simplified 2D model of a ventilated PV solar air collector was developed and a model of the solar water collector was presented. These models are based on a nodal approach. The gradient temperature through the layers along the collector's width of collector is assumed to be negligible, the air gap is discretized through the collector length and the temperature, at each node, can be considered as a mean temperature. Chow [36] developed a model, implementing the explicit dynamic model of a hybrid collector, suitable during periods of fluctuating irradiance or intermittent fluid flow. It is a finite difference approach for a hybrid water heating PV module. A multiphysics, finite element computational model for a hybrid concentrating photovoltaic/thermal (CPV/T) water collector was developed by Xu et al. [37] to calculate the thermal and electrical efficiencies of the collector at different water flow rates. Fountenault and Gutierrez [38] developed a model of a system consisting in a rectangular aluminium box on the rear side of the PV module, where water flowed. The hybrid model was implemented using COMSOL Multiphysics software. In their work the simulations were carried through under several assumptions: the solar irradiance is constant, the solar irradiance not used to produce electricity is converted into waste heat, at the inlet the coolant water has uniform and constant temperature.

In this paper the investigation is focused on TESPI panel. It consists in superimposing a layer of water, flowing in a polycarbonate box (see **Fig. 1**), on the PV

panel in such a way to absorb infrared radiation, with a reduced absorption of the visible part of the spectrum [39]. The rear part of the panel is covered with a layer of polyurethane in order to limit heat loss. Multi-layer thermal modelling of the PV module is developed in Tina et al. [30, 31, 40] study: it allows not only to calculate more precisely the PV cell temperature, but also to evaluate both front and back layer temperatures. The numerical results put also in evidence the uncertainties introduced by the environmental variables (ambient temperature, irradiance, wind speed) measurements.

Fig. 1 Exploded view of TESPI panel

2. PV/T MODEL AND ARRANGEMENT

The thermal model for TESPI panel, described in this paper, is implemented in RadTherm environment, an advanced Thermal Analysis Software tool [41]. Thermal models in RadTherm are organized into a hierarchical arrangement of nodes, elements, parts and assemblies. The energy balance is based on combination of radiation, convection and conduction. Imposed heat flux can be added as a function of time as well as time dependent temperatures for boundary conditions. Environmental effects are also included as boundary conditions. The thermal analysis software Radtherm performs the energy balance between the radiative, conductive, convective and auxiliary heat rates based on a surface mesh. Each element in the mesh shows two sides (front and back) separated by a specified thickness. Each surface has an associated thermal node. The energy equation is then discretised by Radtherm using the Crank-

Nicholson implicit finite difference scheme, which is second-order accurate in time and space [42].

Two different water flow rates have been analysed to determine the impact on the cooling of the panel, heat gained and electrical efficiency. RadTherm allows considering a variable solar irradiance and variable weather conditions (ambient temperature, wind speed and wind direction); therefore simulations have been performed taking into account real environmental conditions.

The hybrid system has been modelled using data from materials used in the work of Rosa Clot et al. [12]. It is assumed that the whole panel is covered by PV cells, with no packing material (material used to fill in gaps between the cells on a panel). The PV cells are commercial grade polycrystalline silicon cells, with electrical efficiency of 13%, that decreases with increasing temperature of 0.45%/°C [1/°C]. In [43] it is shown that the maximum power point coefficients are mainly between -0.4 and -0.45 %/°C, modules of thin film technologies have better coefficient than silicon crystalline technologies, among which the CIS technology presents the best thermal performance. The cooling water flows on the front of the collector into a pattern in a polycarbonate box. The back of the panel is insulated by a polyurethane sheet: this normally should increase the PV temperature with negative effect on its efficiency, but in TESPI panel the temperature of PV cells is controlled by water flux. Two prototypes with the same exposed surface have been investigated: vertical configuration and horizontal configuration. Vertical and horizontal configuration are represented in **Fig. 2**.

Fig. 2 TESPI panel configurations: a) vertical and b) horizontal

The box has a series of slabs that generate channels for the water flux. This structure has a double function: it increases the mechanical resistance of the box, avoiding the bumping of the box itself; it allows a control of the temperature distribution on the collector. A scheme of the cross section of the assembly is shown in **Fig. 3**.

Fig. 3 TESPI panel – cross view section

Some assumptions have been made regarding the PV/T panel thermal model, atmospheric conditions, water flow characteristics and other factors, that impact thermal analysis of the system. These assumptions are needed to simplify the thermal model and the representation of operating conditions and modality of installation of TESPI panel:

1. The whole panel is covered by PV cells, with no packing material;
2. The effect of the variability of spectral irradiance is negligible;
3. Water at the inlet of the PV/T reservoir has uniform and constant temperature for each seasonal simulation;
4. No dust is deposited on the PV/T surface;
5. The junction between polycarbonate box and PV panel is perfectly adhering;
6. The direction of wind is perpendicular to the exposed face of the panel

Hybrid collector is located at the latitude of Lecce (South of Italy) oriented with the face towards South with a tilt of 30°. It's ground mounted without external shading. Data are available about solar radiation, air temperature, and wind speed hourly from

1999 to 2003. The data were collected by a weather station, installed on the buildings of the Department of Engineering for Innovation of University of Salento (Lecce).

3. THEORY AND GOVERNING EQUATIONS

The mathematical model is based on the energy balance between the environment and the TESPI system. The energy balance considers the total irradiance, that is according CEI EN 60904-3 the total radiant power incident upon unit area of an inclined surface in $W \cdot m^{-2}$, incident on the plane of the collector, the optical losses, the thermal losses and the thermal energy subtracted by the heat transfer fluid, used within the box of polycarbonate. The predictive mathematical model is fundamental to ensure the correct correlations be implemented in simulation software, to identify the terms of the energy balance, depending on the type and conditions of the collector, the optical properties and the environmental conditions. All three modes of heat transfer are involved: conduction, convection, radiation. Heat transfer by conduction to the panel structural framework is often ignored because of the small area of contact points and junctions; however, it is considered throughout the RadTherm simulations from the TESPI panel surface. Steady state heat conduction is given by Equation (1):

$$\nabla \cdot \left(k \nabla T \right) = 0 \tag{1}$$

A part of solar energy, incident on the solar collector, is absorbed by the polycarbonate sheet ($q_{sol-plc}$). The radiation transmitted by the polycarbonate box ($q_{sky,rad}$) is absorbed by the heat transfer fluid in the infrared field. Heat transfer fluid

receives heat by convection, also due to the heat removed from the PV cells of the panel. Part of the heat generated in the conversion into electric energy is transferred to the heat transfer fluid by conduction through the glass of the photovoltaic panel and the base of the polycarbonate box. The remaining part of energy is retransmitted back from the top the panel by convection and radiation U_f, as well as by the back of the panel U_b and heat loss through thermal bridges at the junctions $U_{los\text{-}bdg}$. A scheme of the layers of TESPI and main energy fluxes is shown in **Fig. 4**.

Fig. 4 Scheme of the layers of TESPI and main energy fluxes

The convective heat transfer between the inner surface of polycarbonate box and the heat transfer fluid is given by Equation (2):

$$q_{cnv} = hA\left(T_2 - T_1\right) \tag{2}$$

In this equation, both temperatures T_1 and T_2 are local variables. To model the convective heat transfer from the inner surface of the box to the heat transfer fluid in case of turbulent flow the Equation (3), locally valid for the flat plate, is used [44]:

$$Nu_x = 0.0296\,\mathrm{Re}_x^{4/5}\,\mathrm{Pr}^{1/3}\begin{pmatrix} 0.6 \le \mathrm{Pr} \le 60 \\ 5\cdot 10^5 \le \mathrm{Re}_x \le 10^7 \end{pmatrix} \tag{3}$$

When the flow on the flat plate is laminar, Equation (4) is used [44]:

$$Nu_x = 0.332\,\mathrm{Re}_x^{1/2}\,\mathrm{Pr}^{1/3}\left(\mathrm{Pr} \ge 0{,}6\right) \tag{4}$$

Equation (5) governs the conductive heat transfer through the walls:

$$q_{cnd} = \frac{Ak\left(T_1 - T_2\right)}{s} \tag{5}$$

In particular thermal power yielded by PV cells is transferred to PV glass and EVA layers and it is given by Equations (6, 7):

$$q_{PV-g} = A\frac{k_g}{s_{gl}}\left(T_{PV} - T_g\right) \tag{6}$$

$$q_{PV-EVA} = A\frac{k_{EVA}}{s_{EVA}}\left(T_{PV} - T_{EVA}\right) \tag{7}$$

Heat transfer through the polyurethane surface, the PV cells and aluminium box photovoltaic panel occurs both by convection and radiation. The mechanism of the convective heat transfer depends on the pressure inside the section that is created between the two surfaces. At low pressures the heat transfer is mainly due to molecular conduction, while at high pressures natural convection is prevalent. Radiation is always present and represents the most important contribution in heat transfer. The two main mechanisms, responsible for the phenomenon, are considered: molecular and natural convection in function of the pressure inside the gap between the two surfaces. Heat transfer by radiation between the two surfaces is calculated through the Equation (8):

$$q_{xy,rad} = \frac{\sigma\left(T_x^4 - T_y^4\right)}{\frac{1-\varepsilon_x}{A_x} + \frac{1}{F_{x\_y}A_x} + \frac{1-\varepsilon_y}{A_y\varepsilon_y}} \tag{8}$$

Between the outside surface and the atmosphere, heat is exchanged for both convection and radiation. The convection can be both natural and forced, depending on the wind. The heat loss by radiation is due to the temperature difference between the surfaces and the sky. Convective heat transfer between TESPI and atmosphere is the

major contributor to heat loss, especially in windy conditions, and it is calculated with Equation (9).

$$q_{amb,cnv} = h_{amb} A\left(T - T_{amb}\right) \tag{9}$$

When the wind speed is not negligible the forced convection is considered. In this case, the Nusselt number is calculated through Zhukauskas formula for forced convection with Equation (10):

$$Nu = \frac{h_{amb} L}{k_{amb}} = C \,\mathrm{Re}_L^m \,\mathrm{Pr}^n \tag{10}$$

Radiative heat transfer, due to the temperature difference between the outer surface and the sky, is evaluated approximating TESPI panel as a small gray and convex surface in a large cavity, approximated as a black body (the sky). The net thermal radiation exchanged is given by Equation (11):

$$q_{sky,rad} = \sigma \varepsilon A\left(T^4 - T_{sky}^4\right) \tag{11}$$

The FEA software being used in this study, RadTherm, considers multimode heat transfer and these results appropriate for this study, because of the not homogeneous temperature field that is created as water flows from the inlet to the outlet of polycarbonate box.

RadTherm numerically solves the continuity and momentum equations, which are the governing equations for the fluid flow as in Equations (12) and (13).

$$\nabla \cdot \left(\rho u\right) = 0 \tag{12}$$

$$\frac{\partial u}{\partial t} + u \cdot \nabla u = -\frac{1}{\rho} \nabla p + \frac{\mu}{\rho} \nabla^2 u \tag{13}$$

The conduction-convection equation is also solved for heat transfer in the flowing water into the polycarbonate box, shown in Equation (14).

$$\rho C_p u \cdot \nabla T = \nabla \cdot \left(k \nabla T\right) \tag{14}$$

The amount of energy converting into electric power in the PV cell is a function of the PV cell efficiency, η_{PV}. It is given by equation (15) below as a function of its efficiency at reference temperature, the PV cell temperature, and the PV cell thermal coefficient [29].

$$\eta_{PV} = \eta_{T_{ref}} \left[1 - \beta_{ref} \left(T_{PV} - T_{ref}\right)\right] \tag{15}$$

In Equation (8), η_{Tref} is the PV cell efficiency at reference conditions (i.e. T_{ref} = 25°C, q_{rad}=1000 W/m^2), and β_{ref} is the PV thermal coefficient.

The software modelled the flow through the polycarbonate box by solving the continuity, momentum, and energy equations. At each time step in the performed simulations, the PV cell efficiency, η_{PV} , is calculated from Equation (15) in a post processing session from the user input values for β_{ref}, η_{Tref}, T_{ref}, and from the RadTherm solved value for the cell temperature, T_{pv}. It has been assumed, using a safe approach, a loss in efficiency for the PV cells of 0.45%/°C, as reported in the analysis of commercial PV modules on the temperature dependence of photovoltaic module electrical performance [28]. Mapping the temperature (time depending) of the PV cells in the case of commercial PV panel and the temperature of the PV cells in TESPI, increase or decrease of the efficiency is estimated. The reference for the comparison has been considered the daily time profile (in its reference month) of the production (for installed

power kWhe/kWp) of a PV module, installed at the same latitude. The reference data have been extracted from the database of a commercial software for the analysis of productivity of a photovoltaic system [41]. Equations (16) has been used to calculate the thermal energy extracted by the coolant water.

$$E_{av} = mC(T_{out} - T_{in}) \tag{16}$$

4. TEST CASES

A test case for the whole year has been simulated in RadTherm, in which water inlet velocity and temperature have been changed in order to determine optimal design conditions for TESPI panel (**Table 1**). The simulations have been carried out considering a flow rate of 0.1 l/min and a flow rate of 0.5 l/min of fluid as the experimental tests performed and considering a wind speed of 1 m/s and 4 m/s. Flow rate of 0.1 l/min has been chosen to test the hybrid collector in conditions close to stagnation. This value of flow rate has the function to protect PV cells from overheating that occurs in stagnation conditions. Flow rate of 0.5 l/min is a typical operating flow rate for a solar thermal collector. The inlet temperature has been set at 20 °C in summer, 10 °C in winter and 5 °C at the equinoxes. This choice has been made taking into consideration the average temperature of water supply network in different season in the year.The solar collector is located at the latitude of Lecce (South of Italy), with a tilt of 30°. However, in order to represent the results, several cases have been chosen just at solstices and equinoxes.

Table 1 Summary of test cases

It was possible to place the thermal model in the desired "Natural Environment", setting the Global Position where the object is placed in the correct location. A summary of properties of materials, taken from RadTherm material database, used to build the PV/T system is shown in **Table 2** and **Table 3**.

Table 2 Material properties – polycarbonate box

Table 3 Material properties – PV panel

The versatility of the simulation model allows, in particular, to change the input data, operating with other geometries or experimenting different materials, in order to optimize the performance of the solar collector. The TESPI model is made up of 46 parts and 4096 shell elements. The method of Crank - Nicholson results the most stable and versatile for solving differential parabolic equations and has a degree of accuracy of the second order in time and space [42].

5. VALIDATION

The validation of the thermal model has been obtained with experimental data acquired during the prototype testing. In **Fig. 5** the temperature, measured by thermocouples at the outlet of TESPI prototype in a clear-sky day of September, solar radiation of 20 MJ/day, flow rate of 0.5 l/min, is reported. With the same test conditions a thermal simulation has been performed.

Fig. 5 Thermal model validation

The error between experimental data and calculated results by RadTherm solving Equations (12, 13, 14) model is represented in **Table 4**.

Table 4 Error – Thermal model/TESPI prototype

The error of electric energy production between measured experimental data and calculated by means of RadTherm model is represented in **Table 5**.

Table 5 Percent error – PV production

6. RESULT AND DISCUSSION

As described in the paragraph 4, although a whole year test case has been simulated, significant days at solstices and equinoxes are graphically reported. The energy gained by the heat transfer fluid in the simulated day is obtained normalizing the energy for unitary surface area exposed. Temperature of the silicon cells of the hybrid panel is compared to the temperature of the cells of the photovoltaic panel without the transparent box and the efficiency of electric conversion gained is obtained by Equation (15). The flow of heat transfer fluid gives a beneficial effect on the temperature of the PV cells because it decreases the temperatures of PV cells. The benefit is appreciable in the cells close to the inlet (Bottom PV cells), while the benefit appears to be less on the cells near the outlet (Top PV cells), because the heat transfer fluid is heated in its serpentine path between baffles. It results that an acceptable approximation is to refer to the average temperature of the PV cells along the module, to compare the efficiency of the PV module of TESPI panel to that of the reference PV module. The variation of outlet water temperature along daytime for horizontal and vertical configuration for a flow rate 0.1 l/min and a flow rate of 0.5 l/min of fluid and average temperature of PV cells are presented respectively in Fig. 6 and Fig. 7 for summer solstice while, in **Fig. 8**, the temperature of polycarbonate sheet along the panel is represented. The variation of outlet water temperature and average temperature of PV cells are reported in **Fig. 9** and

Fig. 10 for autumnal equinox; **Fig. 11** and **Fig. 12** for winter solstice; **Fig. 13** and **Fig. 14** for spring equinox. Available thermal energy and PV gained efficiency are reported respectively in **Table 6** and Table 7 for summer; **Table 8** and Table 9 for autumn; Table 10 and Table 11 for winter; Table 12 and Table 13 for spring.

Case 1 – 4

Fig. 6 Thermal simulation summer solstice – T_{out}

As described in the previous section, in summer season the entering water temperature has been set at 20°C. Outlet temperature curves have an increasing trend in the early part of the day and during the central hours of the sample day, when there is an average solar radiation of 1000 W/m^2 , an air temperature in the range of 29 – 32°C. The curves reach a maximum in the early afternoon and a decay until sunset. The highest temperature reported is 50.9°C, corresponding to vertical configuration, with water flow rate of 0.1 l/min; outlet temperature in the same conditions of water flow rate for horizontal configuration is 45.7°C. When water flow rate is set at 0.5 l/min, the curve has a peak value in the horizontal configuration at a temperature of 42.3°C, while the corresponding vertical configuration presents a maximum temperature of 38.0°C. Temperature gradient between inlet and outlet is larger for vertical configuration because the serpentine path between baffles has more passages along the panel. As reported in **Fig. 8**, on the other hand, the temperature of polycarbonate sheet along the panel is more uniform for horizontal configuration. For this reason, for both values of water flow rate, maximum of water temperature is shifted of around one hour, compared with the corresponding vertical configuration. As reported in **Table 6**, vertical

configuration is the best choice for low flow rate, while horizontal configuration has the highest value of available energy, 3.20 kWh/m^2.

When the wind speed is set at 4 m/s, the highest temperature reported is 45.9°C, corresponding to vertical configuration and water flow rate of 0.1 l/min; outlet temperature in the same conditions of flow rate for horizontal configuration is 42.8°C. For flow rate of 0.5 l/min, the maximum of water temperature for horizontal configuration is 39.4°C, while for the corresponding vertical configuration is 36.4°C. As reported in **Table 6**, also when the wind speed is set at 4 m/s vertical configuration is the best choice for low flow rate, while horizontal configuration has the highest value of available energy, 3.02 kWh/m^2.

Fig. 7 Thermal simulation summer solstice – PV cells temperature

Fig. 8 Thermal simulation summer solstice – temperature profile of TESPI

The curves, reported in **Fig. 7**, show the trend of the average temperature of the cells of the photovoltaic collector hybrid panel, compared to the temperature of the cells of the photovoltaic panel without the coolant action of water. The electric conversion efficiency of the PV cells depends on their operating temperature, less the cells temperature is, higher their PV efficiency is. The highest temperature of the cells, in the case of a water flow rate of 0.1 l/min, is 52.7°C for the vertical configuration and 51.2°C for the horizontal configuration. Setting a water flow rate of 0.5 l/m, the temperature of the cells decreases at 44.9°C for the horizontal configuration and at 39.3°C for the vertical configuration, with a significant benefit in terms of PV efficiency (Table 7), respectively 5.21 and 6.54%.

When the wind speed is 4 m/s, the highest temperature of the cells, for a water flow rate of 0.1 l/min, is 49.9°C for the vertical configuration and 49.6°C for the horizontal configuration, while for a water flow rate of 0.5 l/m, the temperature of the cells is 42.4°C for the horizontal configuration and at 38.2°C for the vertical configuration. The benefit in terms of PV efficiency (Table 7), compared to the PV module at the same environmental conditions (solar irradiance, ambient air temperature, wind speed of 4 m/s) is respectively 3.87% and 4.77%.

Table 6 Thermal performance – summer solstice

Table 7 PV gained efficiency – summer solstice

Case 5 – 8

Fig. 9 Thermal simulation autumnal equinox – T_{out}

Differently from simulations during summer season, though having the same geometry, outlet temperature curves, as reported in **Fig. 9**, reach a lower level of values since the corresponding weather file allocates an average radiation of 850 W/m^2 at 12 am, an ambient air temperature of 27°C and an entering water temperature of 15°C. The highest reported temperature is 41.6°C for vertical configuration, with a water flow rate of 0.1 l/min; outlet temperature for horizontal configuration is 37.8°C. The difference of temperature of the peaks between vertical and horizontal configuration is lower, as it is the difference of available energy. It is evident in **Table 8** and it is also valid when a flow rate of 0.5 l/min is set. In this case the curve reaches the maximum value in the horizontal configuration at 33.1°C, while the corresponding vertical configuration presents a maximum of 30.8°C. Horizontal configuration has the highest value of

available energy, 2.25 kWh/m^2, but the difference with vertical configuration is very small. The reported peak temperature is 39.4°C for vertical configuration and 33.2°C for horizontal configuration, with a water flow rate of 0.1 l/min. When a flow rate of 0.5 l/min is set, the maximum value of temperature in the vertical configuration is 29.1°C, while the corresponding horizontal configuration presents a maximum of 28.6°C. Horizontal configuration has a value of available energy of 2.12 kWh/m^2, and vertical configuration of 1.94 kWh/m^2 .

Fig. 10 Thermal simulation autumnal equinox – PV cells temperature

In Fig. **10** the peak temperature of PV cells, for a water flow rate of 0.1 l/min, is 41.7°C for the vertical configuration and 37.9°C for the horizontal configuration. If water flow rate is 0.5 l/min then the maximum temperature is 32.9°C for the horizontal configuration and 30.7°C for the vertical configuration. The PV efficiency gained is reported in Table 9: there is not a significant difference for low water flow rate, whereas vertical configuration results the best choice with an increased efficiency of 6.03% unlike 5.26% of horizontal configuration.

The temperature of PV cells, for a water flow rate of 0.1 l/min, is 39.7°C for the vertical configuration and 34.9°C for the horizontal configuration; for a water flow rate of 0.5 l/min the maximum temperature is 30.2°C for the horizontal configuration and 29.8°C for the vertical configuration. The PV efficiency reported in Table 9 shows that vertical configuration has an increased efficiency of 4.98% and horizontal configuration of 4.37%.

Table 8 Thermal performance – autumnal equinox

Table 9 PV gained efficiency– autumnal equinox

Case 9 – 12

Fig. 11 Thermal simulation winter solstice – T_{out}

The entering water temperature has been set at 10°C, as typically the temperature of water from the piping network is. During the winter period the thermal energy collected, even for a commercial thermal solar collector, is very low. There is a not very substantial tendency towards vertical configuration (Table 10), but essentially it is very difficult to deduce a trend of the outlet temperature curves (**Fig. 11**) both for a wind speed of 1 m/s and 4 m/s. It is a reasonable assertion that, for the lacking of solar radiation, this behaviour represents the field of uncertainty of the TESPI thermal model.

Fig. 12 Thermal simulation winter solstice – PV cells temperature

The tendency of PV curves (**Fig. 12**) reflects the observations made for the uncertainty of the model in the winter season, even as regards to the efficiency gained for PV panel (Table 11), in any case, very small.

Table 10 Thermal performance – winter solstice

Table 11: PV gained efficiency– winter solstice

Case 13 – 16

Fig. 13 Thermal simulation spring equinox – T_{out}

The entering water temperature has been set at 15°C. The tendency of outlet temperature curves has the same shape seen for summer and autumnal seasons. The maximum value of temperature reported is 38.4°C for vertical configuration, with a water flow rate of 0.1 l/min, for horizontal configuration it is 36.4°C. During spring

season the difference between the maximum of the curves between vertical and horizontal configuration is comparable with autumnal simulations and thus the available energy for water flow rate of 0.1 l/min (Table 12). Whereas, setting a water flow rate of 0.5 l/min, there is a small difference between vertical and horizontal configurations in terms of temperature and available energy. In this case the curve reaches the maximum value in the horizontal configuration at 27.8°C, while the corresponding vertical configuration presents a maximum of 27.5°C.

In the simulations where a wind speed of 4 m/s is set the value of temperature reported is 34.0°C for vertical configuration, with a water flow rate of 0.1 l/min, and 27.6°C for horizontal configuration. Whereas, for a water flow rate of 0.5 l/min the curve reaches in the horizontal configuration the water temperature of 24.5°C, while in the corresponding vertical configuration of 25.7°C.

Fig. 14 Thermal simulation spring equinox – PV cells temperature

The maximum temperature of the PV cells for a water flow rate of 0.1 l/min is 38.9°C for the vertical configuration and 37.9°C for the horizontal configuration. If the entering water flow rate is set at 0.5 l/min, the highest average temperature of the cells is 31.3°C for the horizontal configuration and 29.5°C for the vertical configuration (**Fig. 14**). The PV efficiency gained is reported in Table 13: there is not a significant difference for high flow rate with an increased efficiency of about 4.5%, whereas vertical configuration has the best performance with an efficiency of 2.71% for low water flow rate.

PV solo curve presents a peak of temperature of about 45°C at noon, with a radiation of 800 W/m^2 and a temperature of 20°C. That is the typical NOCT value for a commercial PV panel and represents an index of reliability for the realized thermal model. The peak temperature of the PV cells for a wind speed of 4 m/s and a water flow rate of 0.1 l/min is 36.1°C for the vertical configuration and 32.1°C for the horizontal configuration. If water flow rate is 0.5 l/min, as reported in Figure 14, the highest average temperature of the cells is 29.0 °C for the horizontal configuration and 28.3°C for the vertical configuration. Both horizontal and vertical configurations present an increased efficiency of about 2.7%, for high water flow rate.

Table 12 Thermal performance – spring equinox

Table 13 PV gained efficiency– spring equinox

The annual performance (per month) of energy yielded by TESPI combined collector in the horizontal and vertical configurations, for water flow rates of 0.1 l/min and 0.5 l/min and wind speed of 1 m/s and 4 m/s is reported in **Table 14**, and in Table 15 as η_g, electric efficiency gained by the PV module in TESPI at the same environmental conditions (solar irradiance, ambient air temperature, wind speed) of a commercial PV module exposed. This evaluation is important in order to determine optimal design conditions for TESPI panel. Indeed, it results that for low water flow rate the temperature gradient between inlet and outlet is wider for vertical configuration, because the coolant water has more transits into the serpentine path between baffles. This configuration permits an efficient distribution of temperature along the panel, while, with regard to horizontal configuration, the system drifts towards a more uniform

field of temperature between inlet and outlet. Available energy for water flow rate of 0.1 l/min and a wind speed of 1 m/s is 238.09 kWh/m^{2}year for horizontal configuration and 142.23 kWh/m^{2}year for vertical configuration. When the wind speed is considered 4 m/s, available energy is 189.29 kWh/m^{2}year for horizontal configuration and 120.62 kWh/m^{2}year for vertical configuration. Efficiency gained by underlying PV panel results 3.09% for the horizontal configuration and 2.26% for the vertical configuration, while for wind speed of 4 m/s is 2.15% for the former and 2.61 % for the last. When a water flow rate is set at 0.5 l/min, typical operating parameter for a flat solar collector, the distribution of temperature along the panel is comparable, as the curve of outlet temperature, for both configurations. Available energy is 691.04 kWh/m^{2}year for horizontal configuration and 675.46 kWh/m^{2}year for vertical one with PV gained efficiency respectively of 4.39% and 4.75% when a wind of 1 m/s is considered, while available energy is respectively 646.59 kWh/m^{2}year and 605.03 kWh/m^{2}year with PV gained efficiency of 3.26% and 3.38%, when the wind speed is 4 m/s.

Table 14 Available energy [kWh/m^2]

Table 15 PV gained efficiency

7. Conclusions

In this work, a conceptual PV/T design was modeled and analyzed using a commercial finite element software for thermal simulations, Radtherm Multianalytics, release 10.5. The hybrid system has been modelled on TESPI panel, consisting in superimposing a layer of water, flowing in a polycarbonate box, on the PV panel. The rear part of the panel is covered with a layer of polyurethane. Two prototypes have

been investigated: vertical configuration and horizontal configuration, considering a flow rate of 0.1 l/min and of 0.5 l/min of fluid, located at the latitude of Lecce (South of Italy), with a tilt of 30°. The inlet temperature has been set taking into consideration the average temperature of water supply network in different seasons in the year. Numerous simulations were completed to model the heat transfer across the TESPI panel and to determine the thermal available energy and PV gained efficiency. Water flow velocity, wind speed and configurations were varied and analyzed to determine which combinations yielded the most useful thermal and electrical output. It was found that the highest thermal available energy and PV gained efficiency were achieved for test cases involving high flow velocity. In this case available energy is 691.04 kWh/m^2 year for horizontal configuration and 675.46 kWh/m^2year for vertical one with PV gained efficiency respectively of 4.74% and 5.44% when the wind speed is set at 1 m/s and 646.59 kWh/m^2year for the former and 605.03 kWh/m^2year for the last with PV gained efficiency respectively of 3.26% and 3.38% in the case of wind speed of 4 m/s The distribution of temperature along the panel is comparable, as the curve of outlet temperature for vertical and horizontal configurations. High inlet flow rates combining with low inlet temperature result in the lowest surface and PV cell temperatures, thus the highest electrical efficiency, but water exiting TESPI panel has not significant temperature change. As the temperature of working fluid in TESPI cannot be the typical temperature of the fluid of a commercial thermal solar collector in order to have any profit for the PV panel, the water exiting the hybrid panel can be used for pre-heating applications. On the other hand, high flow rates would require larger pumps, thus more

electrical power, depending on the size of the panel array, which may reduce the electrical gains obtained in such a system. A cost savings study would be required to determine the optimal balance of electrical efficiency and available thermal energy.

ACKNOWLEDGMENT

This work has been possible tanks to the funding of Italian Ministry of "Ambiente e della Tutela del Territorio e del Mare" (Ministry decree Prot. SEC DEC 2011 000322 of 5th April 2011).

NOMENCLATURE

A	surface area [m^2]
a	available
amb	ambient air
avg	average
B	back of panel
bdg	thermal bridge and junction
C	specific heat [J $kg^{-1}K^{-1}$]
cnd	conductive heat transfer mode
cnv	convective heat transfer mode
EVA	EVA layers
F	front of panel

F_{i_j}	view factor
G	solar radiation [Wm^{-2}]
g	gained
gl	glass
h	heat transfer coefficient [$Wm^{-1}K^{-1}$]
In	inlet
inc	incident
K	thermal conductivity [$Wm^{-1}K^{-1}$]
L	characteristic length [m]
los	thermal loss
Nu	Nusselt number
out	outlet
P	pressure [Pa]
Pr	Prandtl number
plc	polycarbonate sheet
PV	photovoltaic panel
q_i	heat i mode [W]
rad	radiative heat transfer mode
Re	Reynolds number

s	width of the i material [m]
sky	sky
sol	solar
T_i	temperature at i node [K]
u	flow velocity [ms^{-1}]
U_i	overall heat transfer coefficient [$Wm^{-2}K^{-1}$]
ε	emissivity
η	efficiency
μ	dynamic viscosity [Pas]
ρ	fluid density [kgm^{-3}]
σ	Stefan–Boltzmann constant [Wm^2K^4]

REFERENCES

[1] Colangelo, G., Favale, E., de Risi, A., Laforgia, D., 2012, "Results of Experimental Investigations on the Heat Conductivity of Nanofluids Based on Diathermic Oil for High Temperature Applications", Applied Energy, **97**, pp. 828-833.

[2] Colangelo ,G., Favale, E., de Risi, A., Laforgia, D., 2013, "A new solution for reduced sedimentation flat panel solar thermal collector using nanofluids", Applied Energy, **111**, pp. 80-93

[3] Colangelo, G., de Risi, A., Laforgia, D., 2006, "Experimental study of a burner with high temperature heat recovery system for TPV applications, Energy Conversion and Management ", **47** (9-10), pp. 1192-1206

[4] Chow, T.T., 2010, "A review on photovoltaic/thermal hybrid solar technology", Applied Energy, **87**, pp. 365-379

[5] Zondag, H.A., de Vries, D.W., Van Helden, W.G.J., Van Zolingen, R.J.C., Van Steenhoven, A.A., 2002, “The thermal and electrical yield of a PV–Thermal collector”, Solar Energy, **72**, pp. 113-128

[6] de Vries, D. W., 1998, Design of a photovoltaic–thermal combi-panel, PHD thesis, pp. 8-12

[7]Kalogirou, S.A., 2001, “Use of TRNSYS for modeling and simulation of a hybrid PVthermal solar system for Cyprus”, Renewable Energy, **23**, pp. 247-60

[8] Kalogirou, S.A., Tripanagnostopoulos, Y., 2006, “Hybrid PV/T solar systems for domestic hot water and electricity production”, Energy Conversion and Management 2006; **47**(18-19), pp. 3368-82

[9] Vokas, G., Christandonis, N., Skittides, F., 2006, “Hybrid photovoltaic-thermal systems for domestic heating and cooling – a theoretical approach”, Solar Energy, **80**, pp. 607-15

[10] Chow, T. T., Pei, G., Fong, K.F., Lin, Z., Chan, A. L. S., Ji, J., 2009, “Energy and exergy analysis of photovoltaic-thermal collector with and without glass cover”, Applied Energy, **86**(3), pp. 310-6

[11] Dubey, S., Tiwari, G. N., 2009, “Analysis of PV/T flat plate water collectors connected in series”, Solar Energy, DOI:10.1016/j.solener.2009.04.002

[12] Rosa-Clot, M., Rosa-Clot, P., Tina, G.M., 2011, “TESPI: Thermal Electric Solar Panel Integration”, Solar Energy, **85**, pp. 2433-2442

[13] Zondag, H. A., De Vries, D. W., Van Helden, W. G. J., Van Zolingen, R. J. C., Van Steenhoven, A. A., 2002, “The thermal and electrical yield of a PV-Thermal Collector, Solar Energy”, **2**, pp. 113-128

[14] Hottel H., Woertz B., 1942, “The Performance of Flate Plate Solar Heat Collector”, Trans ASME, **64**, pp. 91-104

[15] Hottel, H., Whillier, A., 1955, “Evaluation of Flat-Plate Solar Collector Performance, Trans Conf Use of Solar Energy Thermal Processes”, Tucson. AZ (USA); pp. 74-104

[16] Bliss, J., 1959, “The derivations of several "plate-efficiency factors" usefull in the design of flate-plate heat collectors”, Sol Energy, **3**(4), pp. 55-64

[17] Duffie, J., Beckman, W., 1991, “Solar Engineering of Thermal Processes”, 2nd ed. New York: Wiley Intercience

[18] Close, D., 1967, “A design approach for solar process”, Sol Energy, **11**(12), pp. 112-22

[19] Wijeysundera, NE., 1978, “Comparison of transient heat transfer models for flat plate collectors”, Solar Energy, **21**(6), pp. 517-21

[20] Morrison, GL., Ranatunga, D. B. J., 1980, “Transient response of thermosyphon solar collectors”, Solar Energy, **24**, pp. 55-61

[21] Fraisse, G., Plantier, C., Achard, G., 2003, “Development and experimental validation of a detailed flat-plate solar collector model”, France 5th French and European TRNSYS User Meeting

[22] Klein, S., Duffie, J., Beckman, W., 1974 “Transient considerations of flat-plate solar collectors”, J Eng Power Trans, **96A**, pp. 109-13

[23] Kamminga, W., 1985 “The approximate temperatures within a flat-plate solar collector under transient conditions”, Int J Heat Mass Transf, **28**(2), pp. 433-40

[24] Butcher, J., 1987, “The Numerical Analysis of Ordinary Differential Equations”, New York: Wiley

[25] Oliva, A., Costa, M., Pérez Segarra, C., 1991, “Numerical simulation of solar collectors: the effect of non-uniformity and nonsteady state of boundary conditions”, Solar Energy, **47**(5), pp. 359-73

[26] Villar, N. M., Lòpez, J. M. C., Muñoz, F. D., Garcìa, E. R., Andreas, A. C., 2009, “Numerical 3D heat flux simulations on flat plate solar collectors”, Solar Energy, **83**, pp. 1086-92

[27] Wirz, M., Roesle, M., Steinfeld, A., 2012, “Three-Dimensional Optical and Thermal Numerical Model of Solar Tubular Receivers in Parabolic Trough Concentrators” ASME Journal of Solar Energy Engineering, **134**, pp. 041012-1/9

[28] Skoplaki, E., Palyvos, J., 2009, “On the temperature dependence of photovoltaic module electrical performance: A review of efficiency/power correlations”, Solar Energy, **83**, 614-624

[29] Jones, A. D., Underwood, C. P., 2001, “A thermal model for photovoltaic systems, Solar Energy”, **70**(4), pp. 349-259

[30] Tina, G.M., Scrofani, S., 2008, “Electrical and thermal model for PV module temperature evaluation”, The 14th IEEE Mediterranean Electrotechnical Conference. Ajaccio (France) May 5-7

[31] Tina, G.M., Abate, R., 2008, “Experimental verification of thermal behavior of Photovoltaic modules”, The 14th IEEE Mediterranean Electrotechnical Conference, Ajaccio (France) May 5-7

[32] Bergene, T., Lovvik, O. M., 1995, “Model calculations on a flat-plate solar heat collector with integrated solar cells”, Solar Energy, **55**, pp. 453-462

[33] Zondag, H. A., de Vries, D. W., van Helden, W. G. J., van Zolingen, R. J. C., van Steenhoven, A. A., 2001, “The thermal and electrical yield of a PV-thermal collector, Solar Energy”, **2**, pp. 113-128

[34] Zondag, H. A., de Vries, D. W., van Helden, W. G. J., van Zolingen, R. J. C., van Steenhoven, A. A., 2003, “The yield of different combined PV– thermal collector designs, Solar Energy”, **72**, pp. 253-269

[35] Assoa, Y. B., Menezo, C., Fraisse, G., Yezou, R., Brau, J., 2007, “Study of a new concept of photovoltaic–thermal hybrid collector”, Solar Energy, **81**(9), pp. 1132-1143

[36] Chow, T. T., 2003, “Performance analysis of photovoltaic–thermal collector by explicit dynamic model”, Solar Energy, **75**, 143–152

[37] Xu X., Meyers, M. M., Sammakia, B. G., Murray B. T., 2012, “Thermal Modeling and Life Prediction of Water-Cooled Hybrid Concentrating Photovoltaic/Thermal Collectors”, ASME Journal of Solar Energy Engineering **, 135**(1), 011010-1/8

[38] Fontenault, B. J., Gutierrez-Miravete, E., 2002, “Modeling a Combined Photovoltaic-Thermal Solar Panel”, Comsol Conference in Boston

[39] Lanzafame, R., Nachtmann, S., Rosa-Clot, M., Rosa-Clot, P., Scandura, P.F., Taddei, S., Tina, G. M., 2010, “Field experience with performances evaluation of a single-crystalline photovoltaic panel in an underwater environment”, IEEE Transactions on Industrial Electronics, **57**, pp. 2492-2498

[40] Tina, G. M., Marletta, G., Sardella, S., 2012, “Multi-layer thermal models of PV modules for monitoring applications” 38th IEEE; Photovoltaic Specialists Conference (PVSC)

[41] www.thermoanalytics.com

[42] Fadugba, S. E., Edogbanya, O. H., Zelibe, S. C., 2013, “Crank Nicolson Method for Solving Parabolic Partial Differential Equations”, IJA2M Vol.1, **3**, pp. 8-23

[43] Braga Jùnior, W., Macêdo, W. N., Pinho, J. T., 2013, “Analysis of characteristic parameters of commercial photovoltaic modules”, ISES Solar World Congress

[44] Cengel, Y. A., 2009, “Introduction to Thermodynamics and Heat Transfer”, **12**, 542-543

Figure Captions List

Table Caption List

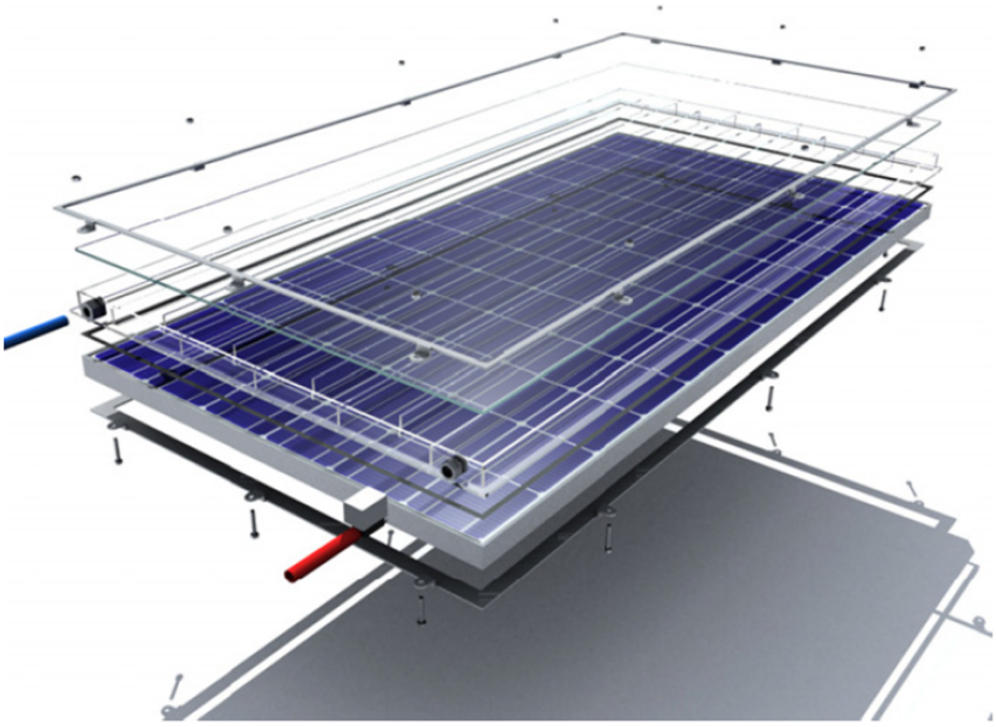

a)

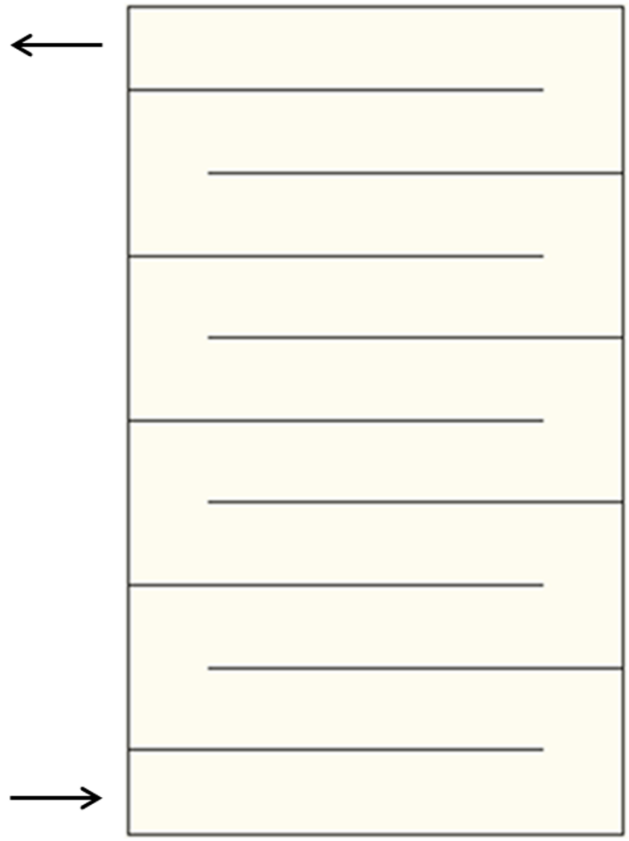

b)

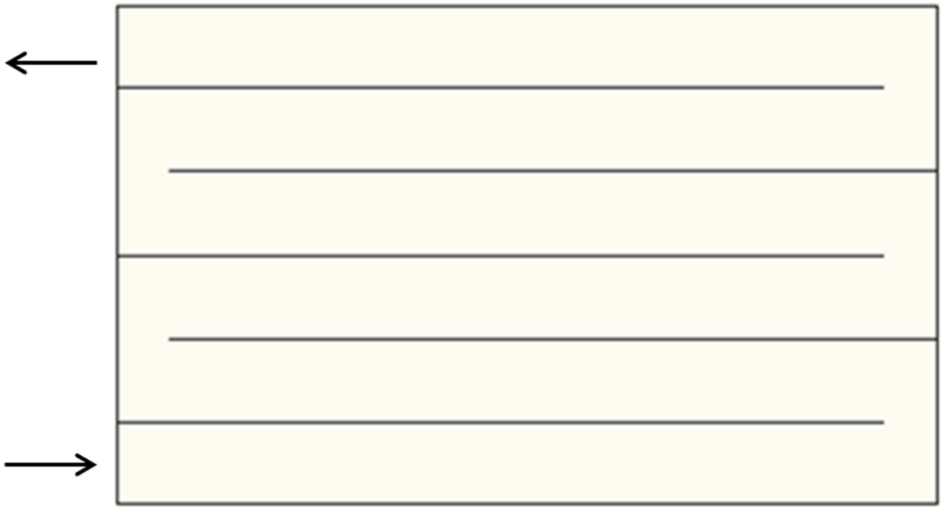

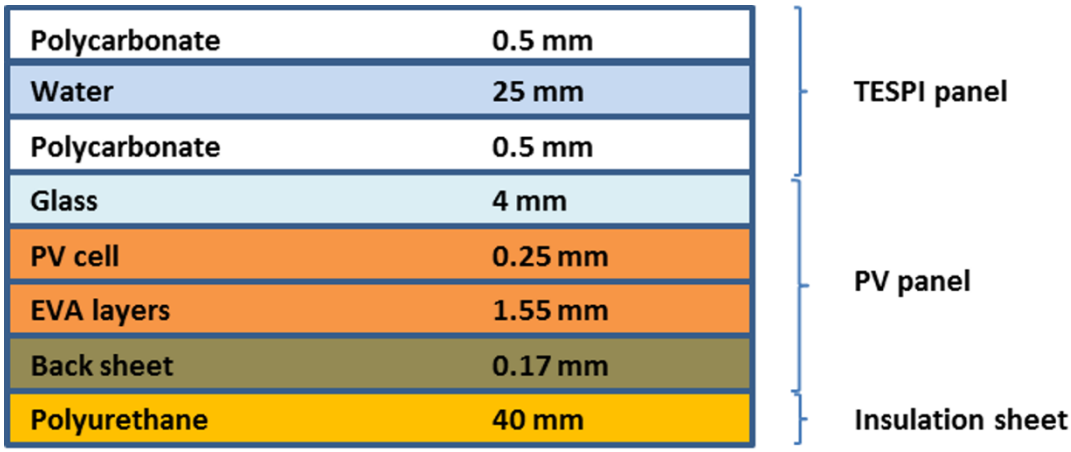
Polycarbonate
0.5 mm
Water
25 mm
Polycarbonate
0.5 mm
Glass
4 mm
PV cell
0.25 mm
EVA layers
1.55 mm
Back sheet
0.17 mm
Polyurethane
40 mm
TESPI panel
PV panel
Insulation sheet

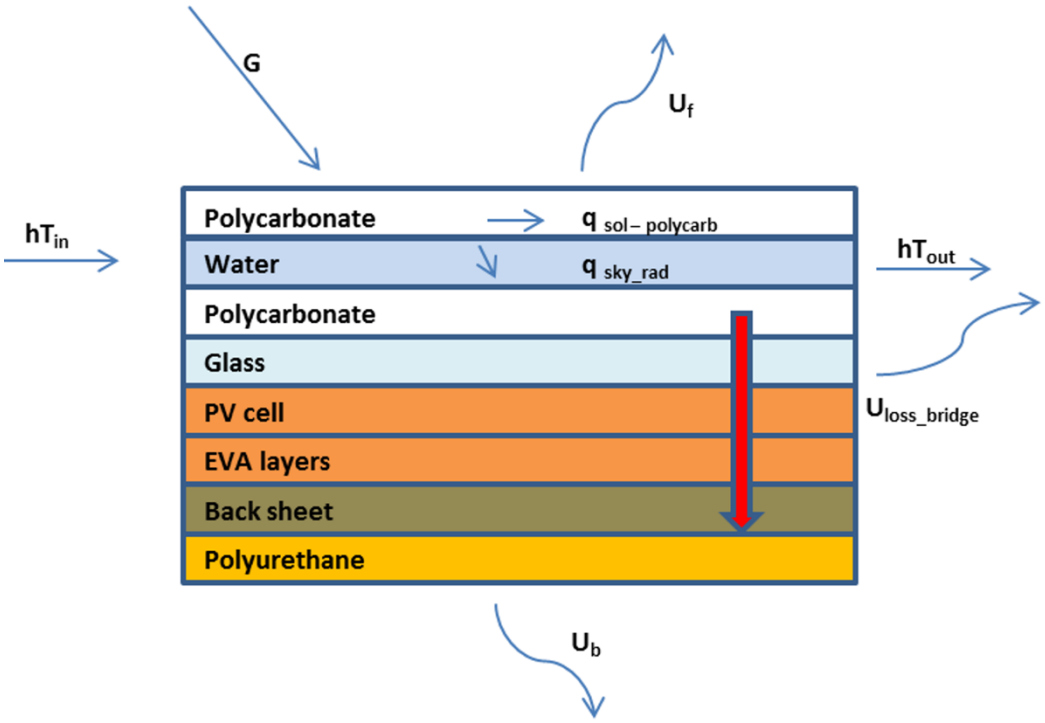
G
U_f
hT_{in}
Polycarbonate
$q_{sol-polycarb}$
Water
q_{sky_rad}
Polycarbonate
Glass
PV cell
EVA layers
Back sheet
Polyurethane
hT_{out}
U_{loss_bridge}
U_b

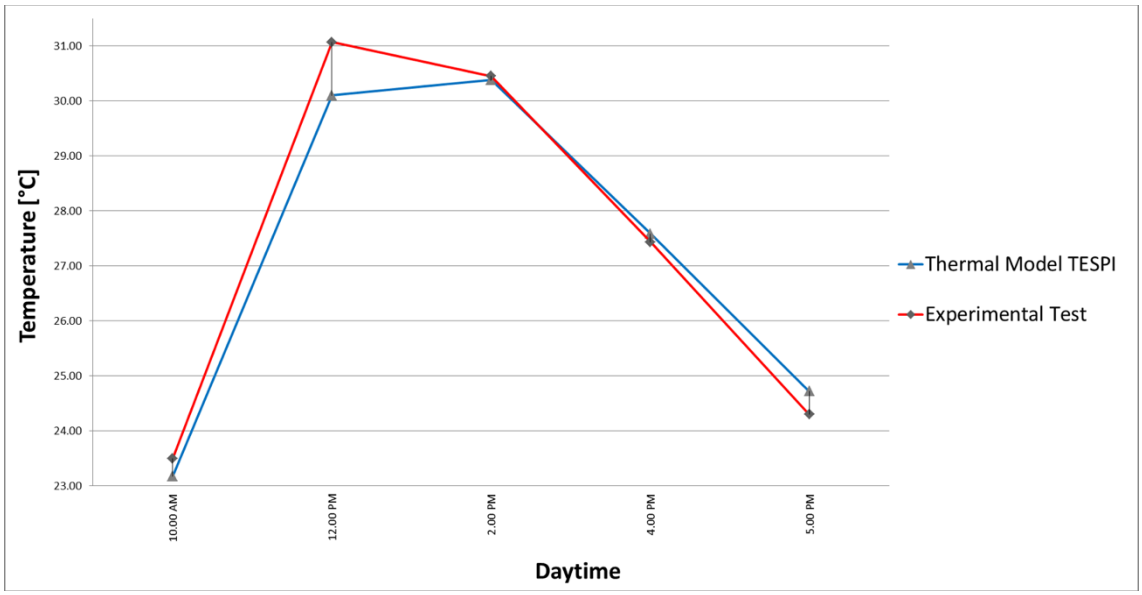
31.00
30.00
29.00
28.00
27.00
26.00
25.00
24.00
23.00
Temperature [°C]
10.00 AM
12.00 PM
2.00 PM
4.00 PM
5.00 PM
Daytime
Thermal Model TESPI
Experimental Test

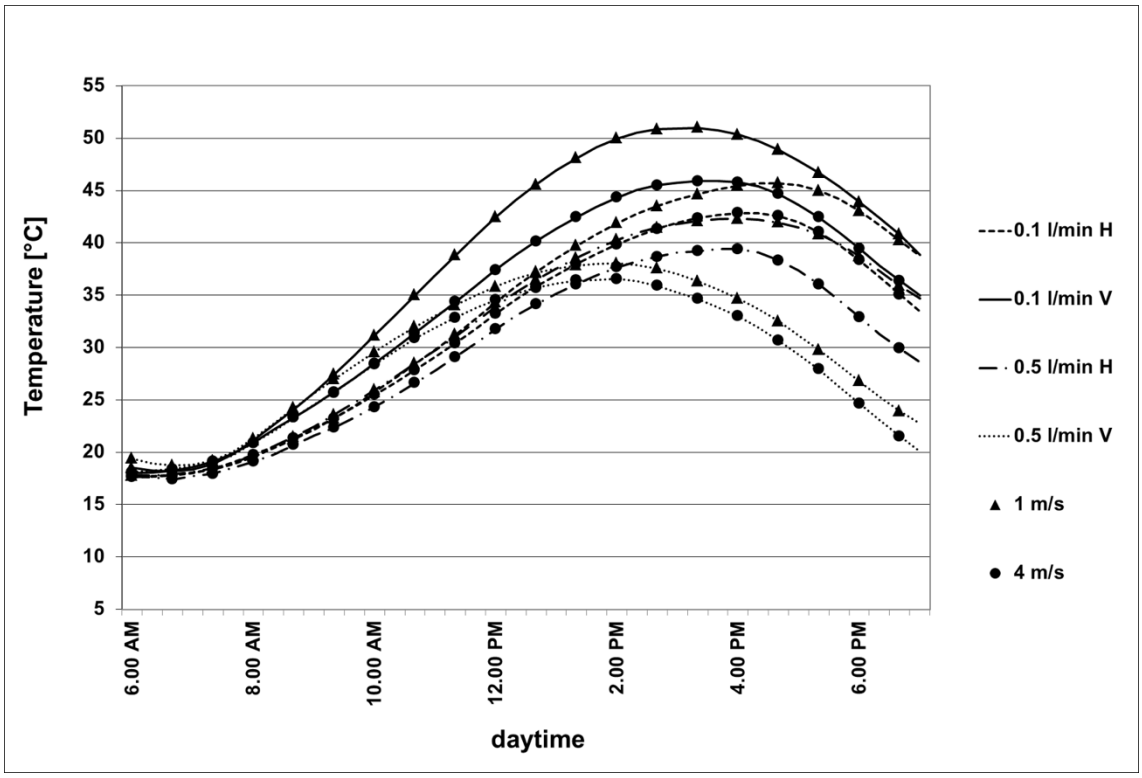
55
50
45
40
35
30
25
20
15
10
5
Temperature [°C]
6.00 AM
8.00 AM
10.00 AM
12.00 PM
2.00 PM
4.00 PM
6.00 PM
daytime
0.1 l/min H
0.1 l/min V
0.5 l/min H
0.5 l/min V
1 m/s
4 m/s

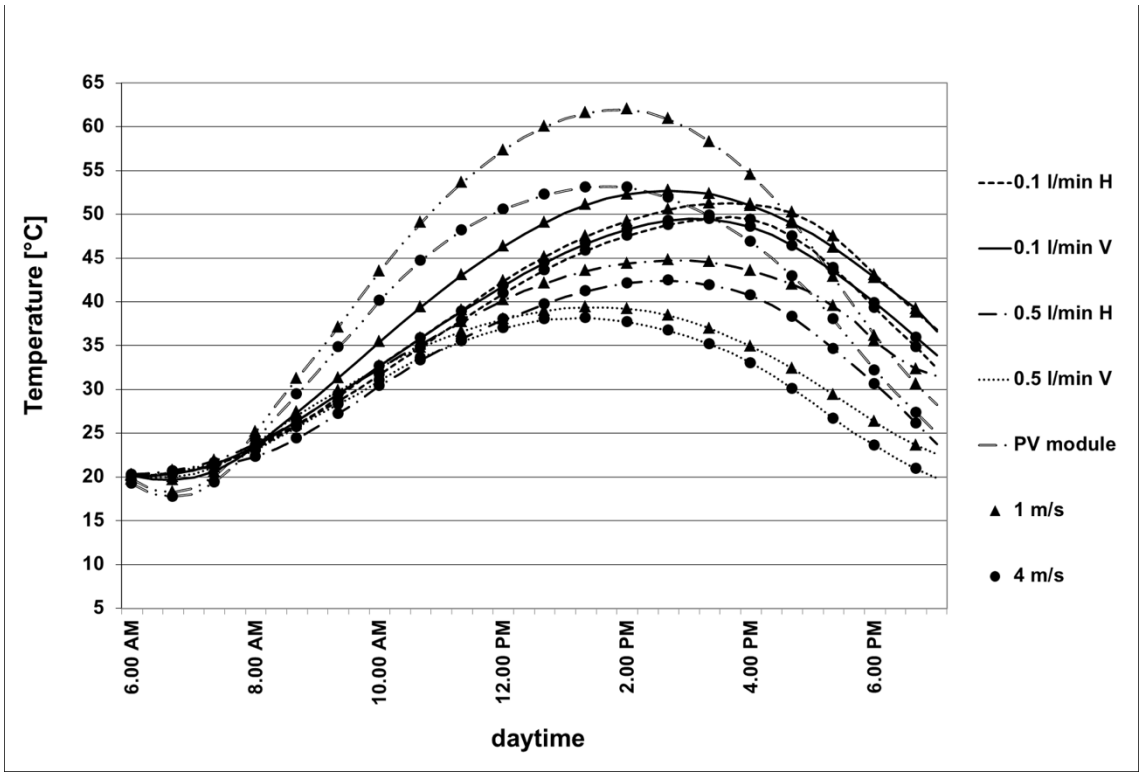
Temperature [°C]
65
60
55
50
45
40
35
30
25
20
15
10
5
6.00 AM
8.00 AM
10.00 AM
12.00 PM
2.00 PM
4.00 PM
6.00 PM
daytime
0.1 l/min H
0.1 l/min V
0.5 l/min H
0.5 l/min V
PV module
1 m/s
4 m/s

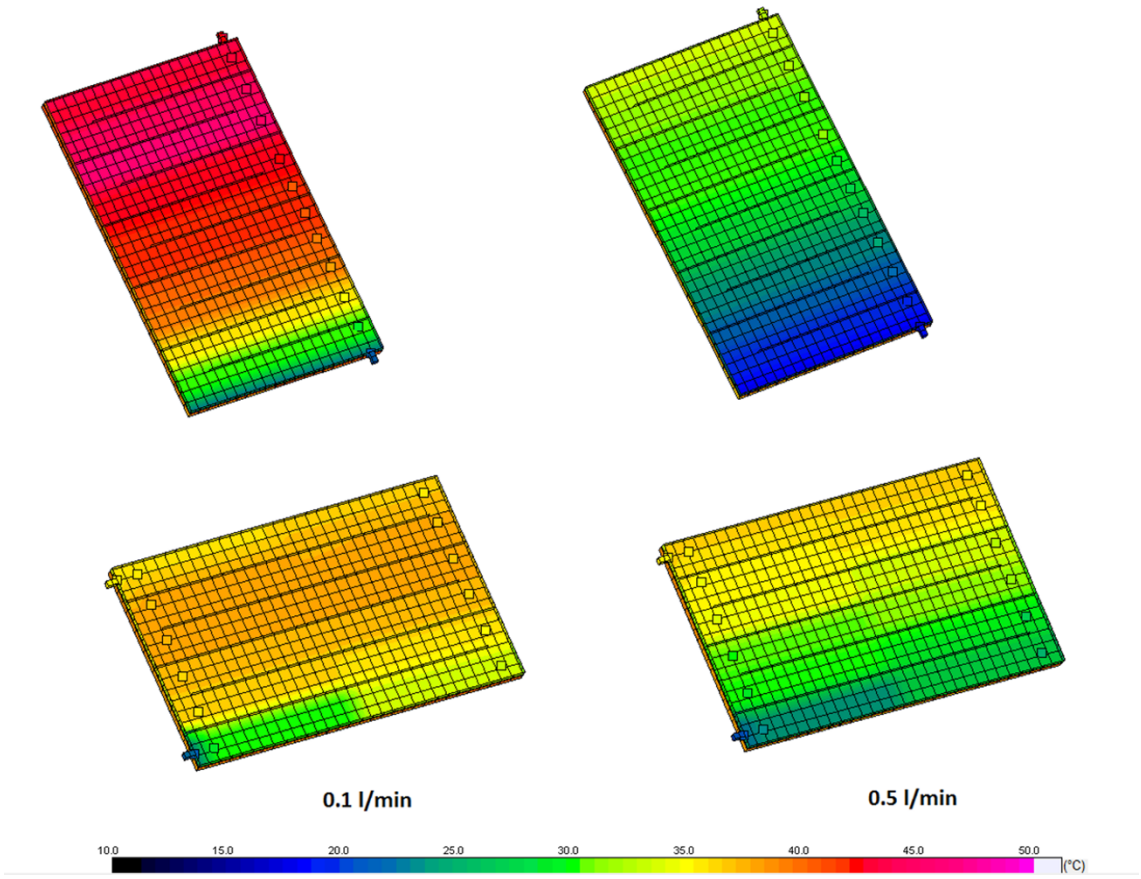
0.1 l/min
0.5 l/min
10.0
15.0
20.0
25.0
30.0
35.0
40.0
45.0
50.0
(°C)

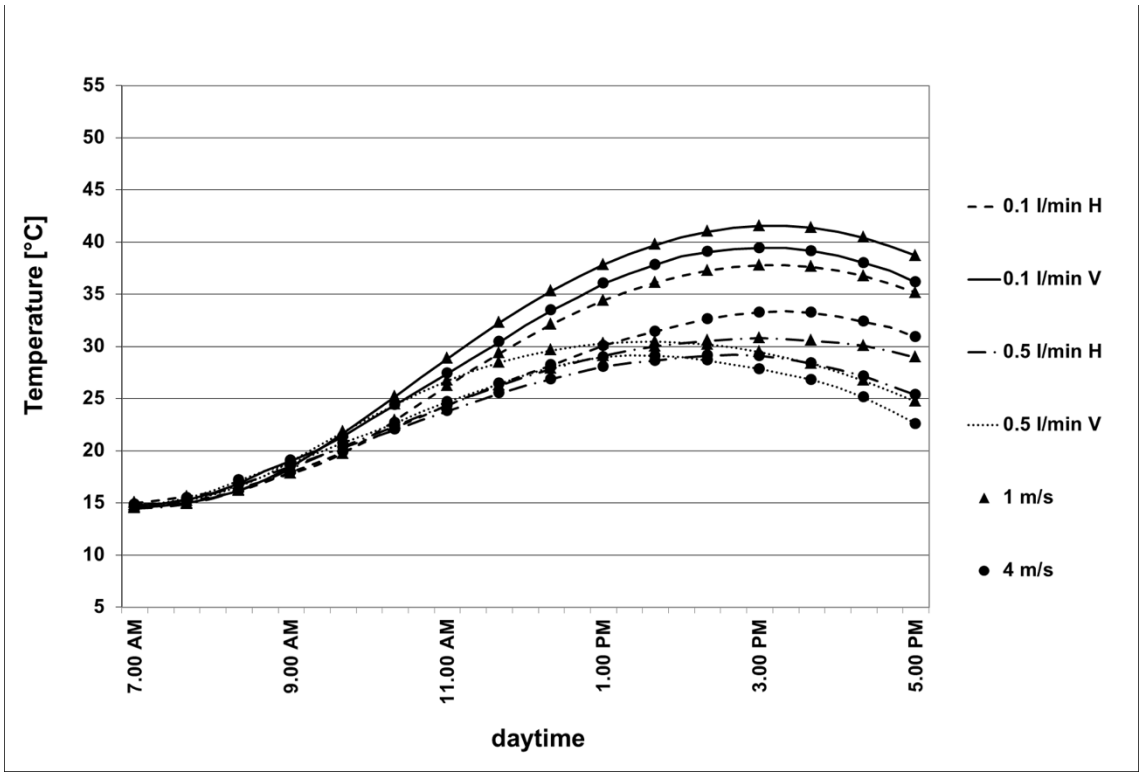
55
50
45
40
35
30
25
20
15
10
5
Temperature [°C]
7.00 AM
9.00 AM
11.00 AM
1.00 PM
3.00 PM
5.00 PM
daytime
0.1 l/min H
0.1 l/min V
0.5 l/min H
0.5 l/min V
1 m/s
4 m/s

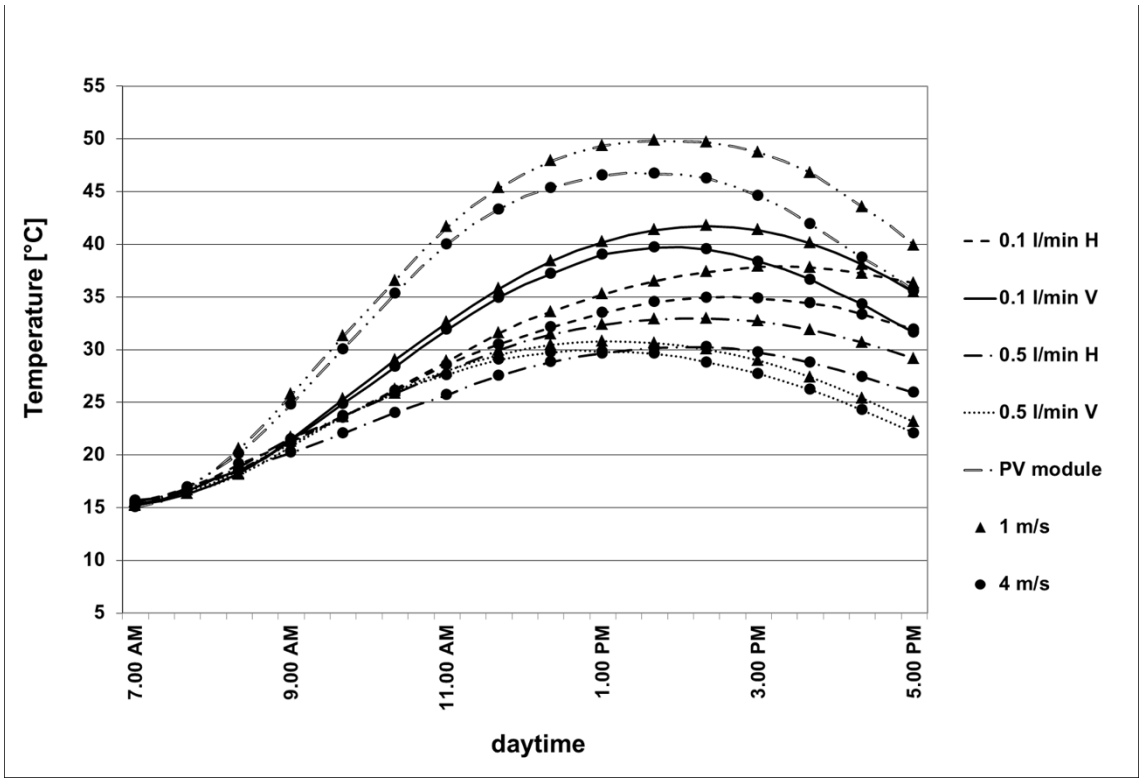
55
50
45
40
35
30
25
20
15
10
5
Temperature [°C]
7.00 AM
9.00 AM
11.00 AM
1.00 PM
3.00 PM
5.00 PM
daytime
0.1 l/min H
0.1 l/min V
0.5 l/min H
0.5 l/min V
PV module
1 m/s
4 m/s

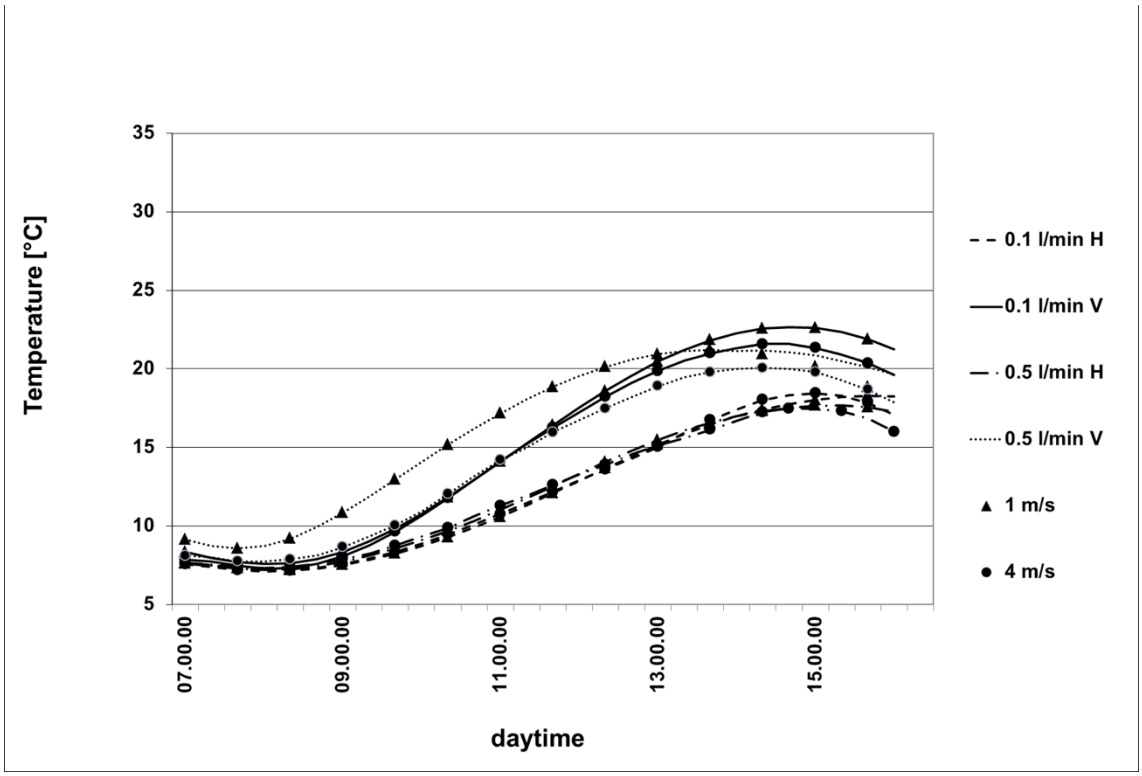
Temperature [°C]
35
30
25
20
15
10
5
07.00.00
09.00.00
11.00.00
13.00.00
15.00.00
daytime
0.1 l/min H
0.1 l/min V
0.5 l/min H
0.5 l/min V
1 m/s
4 m/s

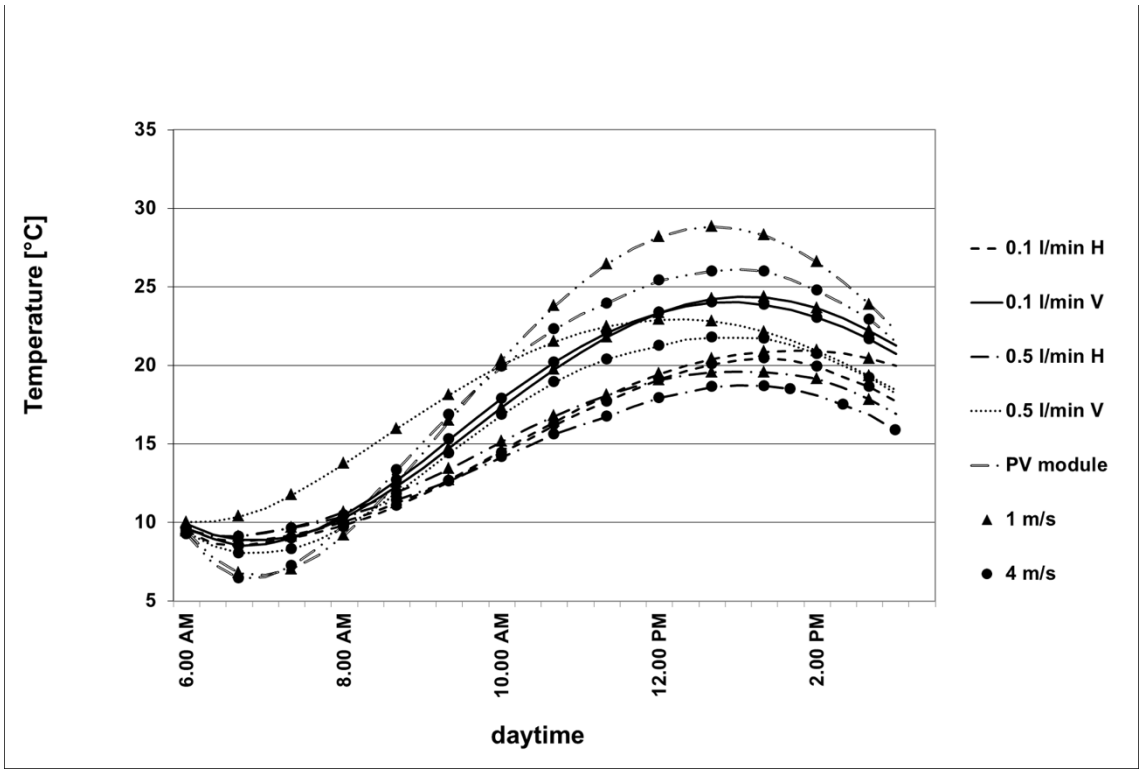
Temperature [°C]
35
30
25
20
15
10
5
6.00 AM
8.00 AM
10.00 AM
12.00 PM
2.00 PM
daytime
0.1 l/min H
0.1 l/min V
0.5 l/min H
0.5 l/min V
PV module
1 m/s
4 m/s

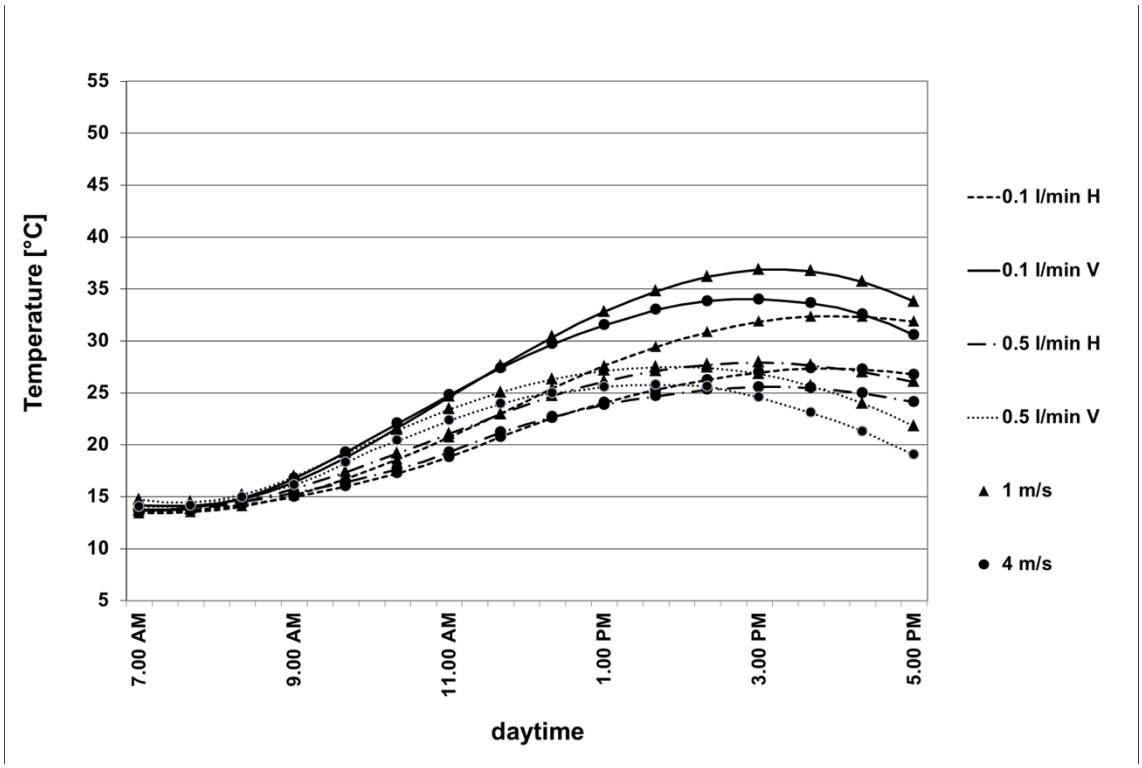
55
50
45
40
35
30
25
20
15
10
5
Temperature [°C]
7.00 AM
9.00 AM
11.00 AM
1.00 PM
3.00 PM
5.00 PM
daytime
0.1 l/min H
0.1 l/min V
0.5 l/min H
0.5 l/min V
1 m/s
4 m/s

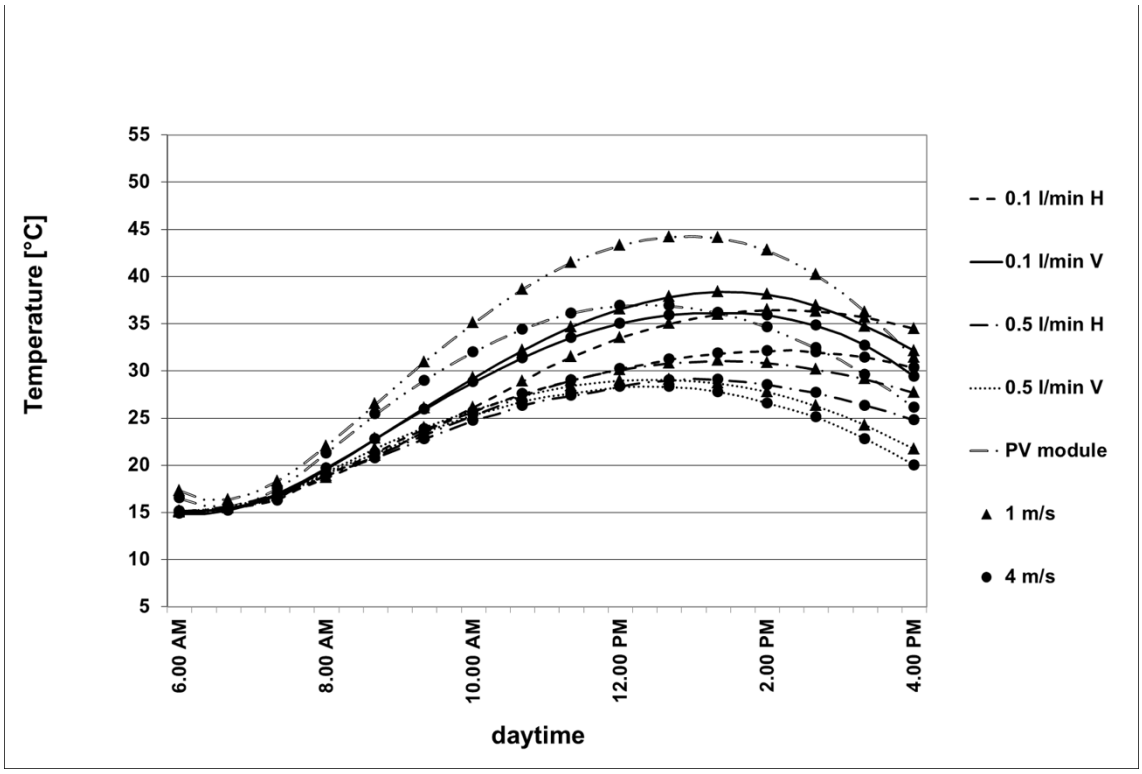
Temperature [°C]
55
50
45
40
35
30
25
20
15
10
5
6.00 AM
8.00 AM
10.00 AM
12.00 PM
2.00 PM
4.00 PM
daytime
0.1 l/min H
0.1 l/min V
0.5 l/min H
0.5 l/min V
PV module
1 m/s
4 m/s

	Period	Configuration	$T_{upstream}$ fluid	Flow rate [l/min]
Case 1	Summer solstice	Horizontal	20°C	0.1
Case 2	Summer solstice	Vertical	20°C	0.1
Case 3	Summer solstice	Horizontal	20°C	0.5
Case 4	Summer solstice	Vertical	20°C	0.5
Case 5	Autumnal equinox	Horizontal	15°C	0.1
Case 6	Autumnal equinox	Vertical	15°C	0.1
Case 7	Autumnal equinox	Horizontal	15°C	0.5
Case 8	Autumnal equinox	Vertical	15°C	0.5
Case 9	Winter solstice	Horizontal	10°C	0.1
Case 10	Winter solstice	Vertical	10°C	0.1
Case 11	Winter solstice	Horizontal	10°C	0.5
Case 12	Winter solstice	Vertical	10°C	0.5
Case 13	Spring equinox	Horizontal	15°C	0.1
Case 14	Spring equinox	Vertical	15°C	0.1
Case 15	Spring equinox	Horizontal	15°C	0.5
Case 16	Spring equinox	Vertical	15°C	0.5

Density [kg/m³]	Conductivity [W/mK]	Specific Heat [J/kgK]	Reflectance	Transmittance
1200	0.2	1300	0.05	0.86

	Type of material	Density[kg/m³]	Conductivity[W/mK]	Specific Heat[J/kgK]	Reflectance	Transmittance
Superior sheet	Glass	2500	0.99	Curve Temp Dep	0.08	0.85
PV cells	Silicon	2330	Curve Temp Dep	Curve Temp Dep	-	-
Insulation sheet 1	EVA	960	0.3	2300	-	-
Insulation sheet 2	Tedlar	1500	0.36	1760	-	-
insulation sheet 3	Polyurethane	1200	0.35	2090	-	-
PV box	Anodized Al	2770	Curve Temp Dep	Curve Temp Dep	-	-

	T_{outlet} Experimental [°C]	T_{outlet} Calculated [°C]	Error %
10:00 AM	23.18	23.5	-1.38%
12:00 PM	30.10	31.1	-3.13%
2:00 PM	30.38	30.5	-0.23%
4:00 PM	27.58	27.4	0.55%
5:00 PM	24.72	24.3	1.73%

	PV production/day Measured [kWh]	PV production/day Calculated [kWh]	Error %
Sample day	1.09	1.1	-0.91%

	Available Energy[kWh/m²]	
Wind	**1 m/s**	**4 m/s**
Case 1	0.85	0.73
Case 2	1.11	0.95
Case 3	3.20	3.02
Case 4	3.07	2.77

	PV gained efficiency	
Wind	**1 m/s**	**4 m/s**
Case 1	4.00%	2.23%
Case 2	3.00%	1.96%
Case 3	5.21%	3.87%
Case 4	6.54%	4.77%

	Available Energy[kWh/m²]	
Wind	**1 m/s**	**4 m/s**
Case 1	0.58	0.49
Case 2	0.71	0.55
Case 3	2.25	2.12
Case 4	2.17	1.94

	PV gained efficiency	
Wind	**1 m/s**	**4 m/s**
Case 1	2.90%	2.70%
Case 2	2.92%	2.60%
Case 3	5.26%	4.37%
Case 4	6.03%	4.98%

	Available Energy[kWh/m²]	
Wind	**1 m/s**	**4 m/s**
Case 1	0.13	0.11
Case 2	0.26	0.20
Case 3	0.63	0.59
Case 4	0.70	0.63

	PV gained efficiency	
Wind	**1 m/s**	**4 m/s**
Case 1	2.28%	1.98%
Case 2	1.15%	0.94%
Case 3	2.47%	2.33%
Case 4	1.26%	1.13%

	Available Energy[kWh/m²]	
Wind	**1 m/s**	**4 m/s**
Case 1	0.42	0.35
Case 2	0.58	0.45
Case 3	1.64	1.54
Case 4	1.78	0.60

	PV gained efficiency	
Wind	**1 m/s**	**4 m/s**
Case 1	2.71%	1.62%
Case 2	1.95%	1.09%
Case 3	4.51%	2.71%
Case 4	4.57%	2.79%

Wind	1 m/s				4 m/s			
	H - 0.1	V - 0.1	H - 0.5	V - 0.5	H - 0.1	V - 0.1	H - 0.5	V - 0.5
Jan	2.99	11.14	13.07	23.34	3.10	7.40	17.67	16.14
Feb	6.12	13.05	22.15	33.22	3.16	9.91	18.87	24.39
Mar	12.69	17.98	50.92	55.27	8.92	16.10	42.77	44.07
Apr	17.94	21.05	65.91	68.90	14.16	20.47	64.13	59.74
May	22.63	25.75	83.59	83.59	18.88	24.89	85.13	75.78
Jun	23.05	29.00	94.49	90.29	19.77	25.59	92.23	80.73
Jul	21.47	34.43	99.30	91.23	18.59	25.31	94.85	83.28
Aug	15.48	27.90	84.88	80.23	13.17	21.35	84.03	75.40
Sep	6.06	21.30	67.50	65.10	8.63	14.33	63.14	59.25
Oct	5.27	16.74	53.82	38.66	4.65	9.30	43.03	43.62
Nov	4.50	11.70	35.88	23.92	4.50	7.20	23.35	26.00
Dec	4.03	8.06	19.53	21.70	3.10	7.44	17.38	16.65
Total	**142.23**	**238.09**	**691.04**	**675.46**	**120.62**	**189.29**	**646.59**	**605.03**

	H - 0.1		V - 0.1		H - 0.5		V - 0.5	
	$\eta_{g\text{-}1\ m/s}$ [%]	$\eta_{g\text{-}4\ m/s}$ [%]	$\eta_{g\text{-}1\ m/s}$ [%]	$\eta_{g\text{-}4\ m/s}$ [%]	$\eta_{g\text{-}1\ m/s}$ [%]	$\eta_{g\text{-}4\ m/s}$ [%]	$\eta_{g\text{-}1\ m/s}$ [%]	$\eta_{g\text{-}4\ m/s}$ [%]
Jan	1.80	1.82	1.42	1,02	3.23	2.42	2.54	1.85
Feb	2.08	1.70	1.68	1.05	3.92	2.56	3.64	2.34
Mar	2.72	1.62	1.95	1.09	4.51	2.71	4.57	2.79
Apr	3.42	1.80	2.21	1.31	4.75	3.02	5.32	3.30
May	3.96	2.05	2.48	1.43	4.95	3.39	5.90	3.86
Jun	4.22	2.23	2.74	1.64	5.13	3.63	6.31	4.40
Jul	4.14	2.42	3.00	1.96	5.21	3.87	6.54	4.77
Aug	3.78	2.58	3.07	2.34	5.19	4.21	6.55	4.92
Sep	3.25	2.70	2.92	2.62	5.02	4.37	6.03	4.98
Oct	2.78	2.55	2.55	2.17	4.58	3.72	4.97	3.82
Nov	2.66	2.30	1.96	1.74	3.83	2.93	3.38	2.45
Dec	2.28	1.98	1.15	0.94	2.47	2,33	1.26	1.13
$\eta_{g\text{-}avg}$	**3.09%**	**2.15%**	**2.26%**	**1.61 %**	**4.39%**	**3.26%**	**4.75%**	**3.38%**